Available online at www.sciencedirect.com
ScienceDirect
International Journal of Thermal Sciences 48 (2009) 372–382
International Journal of Thermal Sciences
www.elsevier.com/locate/ijts

The Discrete Boundary Resistance method for thermal analysis of solid-state circuits and devices

V. Feuillet [a,b,1], Y. Scudeller [b,*], Y. Jarny [a]

[a] *Université de Nantes, Ecole polytechnique, LTN, La Chantrerie, Rue Christian Pauc, BP 50609, 44306 Nantes Cedex 3, France*
[b] *Université de Nantes, Ecole polytechnique, LGMPA, La Chantrerie, Rue Christian Pauc, BP 50609, 44306 Nantes Cedex 3, France*

Received 13 December 2007; received in revised form 18 April 2008; accepted 16 May 2008

Available online 20 June 2008

Abstract

This paper presents a method developed for determining temperature distribution in a semi-analytical way within tri-dimensional solid-state circuits and packaged devices in steady state conditions. The method is an efficient route to investigate large ranging sized structures with an arbitrary complex layout composed of multiple material layers and localized heat sources.

The method, called the Discrete Boundary Resistance (DBR), consists in decomposing the structure into layers of different sizes to develop the temperature solution as a Double Fourier Series after subdividing the contact boundaries into discrete elements. The solution is expressed as a function of thermal resistance attached to the contact boundaries connected to a temperature reference. The performance of the method has been studied in regards with a three-dimensional device involving a non-uniform distribution of voids between layers. Computational time was found to be shorter than ones achieved with the Finite Element method.

Keywords: Thermal modeling; Solid-state circuits and devices; Computational methods; Compact modeling

1. Introduction

Thermal management is a major issue in design of integrated circuits and packaged devices. It is recognized that temperature has a strong influence on reliability. Thermal gradients and coupling effects, caused by localized power dissipation, can drastically affect the performance of the devices [1]. Consequently, analysis achieving an optimal control in temperature is required by considering all involved relevant features such as the operating conditions, the physical properties and structural characteristics of the devices.

Temperature of circuits and packaged devices can be managed by layout optimization, substrate thinning, incorporation of heat spreaders and thermal vias. Investigation is therefore quite complicated because of the nature of three-dimensional heat spreading effects and the existence of non-linear behaviour. It has become essential to obtain simulation tools determining the temperature distribution as a function of device topology, layout, properties of the materials and input power. Among the methods for performing simulations, numerical methods, such as finite elements [2], boundary elements [3,4], are recognized as flexible with the capability to take into account all relevant features of structures. The computational cost of these methods can be extremely high for simulation of complex systems that need dense meshes to obtain acceptable accuracy. Precise thermal simulations can be sometimes virtually impossible as for example for certain Radio-Frequency and microwave tri-dimensional devices that have extremely small heat sources and multiple layers over a wide range of dimension. Analytical and semi-analytical methods become attractive as well for simulations using compact modeling because meshing is not required. Among these methods, one can mention the Green functions [5] and the Integral Transform technique, especially using Fourier series expansions [6,7]. Nowadays, investigation of heat transport in devices with a large range of component sizes remains a challenge and improvements of

* Corresponding author.
E-mail address: yves.scudeller@univ-nantes.fr (Y. Scudeller).
[1] Université Paris 12, CERTES, 94010 Creteil, France.

1290-0729/$ – see front matter
doi:10.1016/j.ijthermalsci.2008.05.011

semi-analytical methods become desirable in terms of flexibility, precision and computational cost.

This paper reports a method called the Discrete Boundary Resistance (DBR) to calculate temperature distribution in a semi-analytical way for tri-dimensional solid-state circuits and devices. The method is an efficient route to investigate complex structures formed with any arbitrary number of compounds and localized heat sources, over a wide range in size. The method, which offers both high precision and reasonable computational cost, is particularly suitable for analysis of compound semiconductor devices that have a strongly non-planar structure with large range of component sizes and a high number of localized heat sources. It could be applicable for example to Radio-Frequency solid-state devices, semiconductor lasers, semiconductor chips, Multi-Chip-Modules, sensors and Micro-Electro-Mechanical-Systems. Most of these devices are constructed of multiple layers having dimensions that can vary from a fraction of a micron to a couple of centimeters. It has already been used to estimate the thermal properties of packaged device [8].

The present method could be considered as a generalization of the approach reported in [9], originally developed to construct thermal compact models for subsystems, in combination with the use of the Fourier Transform technique.

The principle of the method is presented. Its performance, in terms of precision and computational cost, is studied with regards to a tri-dimensional multi-layered device. The case of imperfect contact between layers due to an arbitrary distribution of voids has been especially investigated.

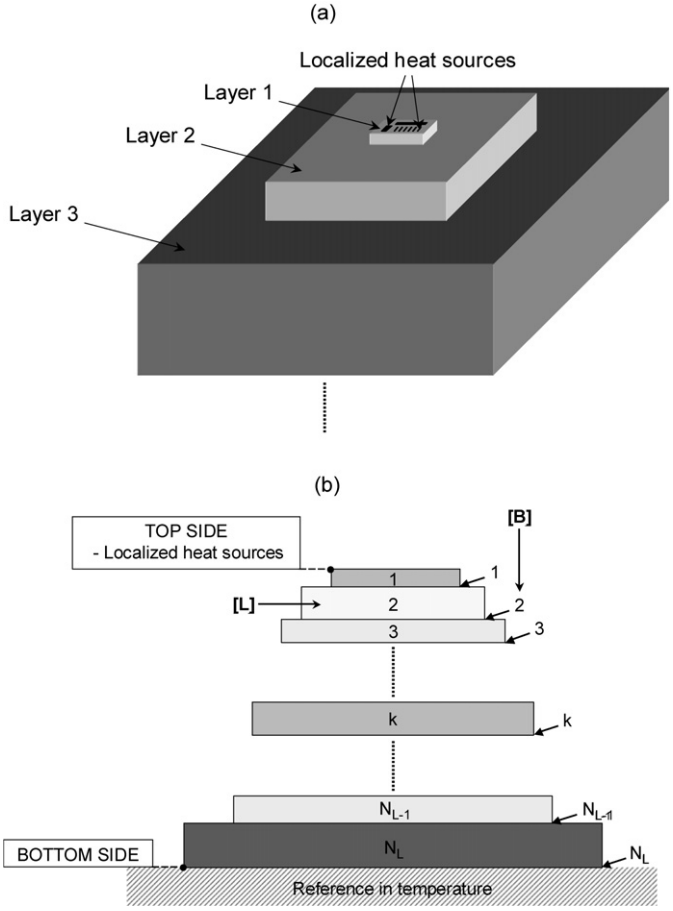

Fig. 1. Layout of a packaged device, as studied, formed with multiple layers of rectangular shapes of different sizes (contacts between layers can be imperfect): (a) three-dimensional view, (b) cross-sectional view ([L]: layer, [B]: boundary contact).

2. The Discrete Boundary Resistance method

Most circuits and packaged devices can be described as a structure of multiple layers of rectangular shapes with different sizes, as illustrated in Fig. 1. The represented structure consists of N_L layers starting from its top side where the N_L-th layer refers to the bottom layer (see Fig. 1(b)). The heat transport mode is heat conduction. Steady state conditions are considered.

For clarity purpose, some simplifications are used. First, the bottom side of the structure should be isothermal and its temperature T_∞ is a reference (zero temperature). Secondly, all faces of the structure in contact with the surrounding medium are adiabatic. In most of cases, the heat exchange by convection and radiation with the surrounding medium can be neglected. Moreover, for convenience, power dissipation is located at the top side of the structure. Additionally, thermal conductivity is constant within each material layer.

Note that the Discrete Boundary Resistance method could be extended to non-isotropic and heterogeneous media with power dissipated at any position of the structure. The method is particularly suitable to take into account imperfect contacts between layers with non-uniform distribution in the plane.

2.1. Principle of the method

The method consists in decomposing the structure into N_L layers of different sizes (Fig. 1) and then in developing for each one the solution of the heat conduction equation after subdividing the contact boundaries into M_C discrete elements, as illustrated in Fig. 2. As demonstrated in the next section, the temperature solution referred to any layer can be expressed in the rectangular coordinate system as a Double Fourier Series satisfying the edge boundary conditions (adiabatic, see Section 2.2). The solution can be then found for the full structure after applying the contact conditions (1) and (3) to any layer as:

– a second type of boundary condition (Neumann) at the top face ($z = 0$), by prescribing an heat flux ϕ over the discrete elements. According to the Fourier law, this condition is written as:

$$-\lambda S^i \left[\left. \frac{\partial T}{\partial z} \right|_{z=0} \right]^i = \Phi^i \tag{1}$$

All quantities refer to the k-th layer and i-th discrete element (surface S), λ is the thermal conductivity of the layer. The different values of ϕ^i describe a spatial distribution such as $\phi^i \equiv \phi^i(x^i, y^i)$ where $i = 1, 2, 3, \ldots, M_C$ and therefore a heat flux vector can be defined as:

$$\vec{\Phi} = \left[\Phi^1, \Phi^2, \ldots, \Phi^i, \ldots, \Phi^{M_C} \right] \tag{2}$$

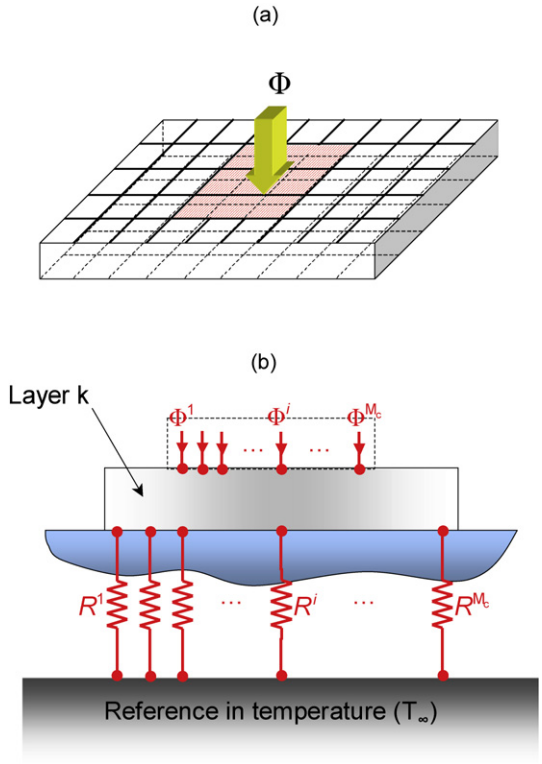

Fig. 2. Arbitrary layer of the layout, as considered by the Discrete Boundary Resistance method: (a) three-dimensional view, (b) cross-sectional view (discrete boundary resistances attached between the bottom face of each layer and the bottom of the entire structure).

– a third type of boundary condition (Fourier) at the bottom face ($z = e$), by defining a thermal resistance R between the discrete element and the bottom side of the structure (zero temperature), as shown in Fig. 2(b). The as defined condition is written as:

$$-\lambda S^i \left[\left.\frac{\partial T}{\partial z}\right|_{z=e}\right]^i = \frac{T^i - T_\infty}{R^i} \tag{3}$$

R^i, expressed in [K W^{-1}], refers to the resistance between the i-th discrete element of the k-th layer and the bottom side of the entire structure. A collection of discrete boundary resistances such as $R^i \equiv R^i(x^i, y^i)$ with $i = 1, 2, 3, \ldots, M_C$ is thus attached to the bottom face of each layer (see Fig. 2(b)). This resistance should be formally considered as the ratio between a temperature difference and the heat flux through the discrete element. It depends on the geometry of the structure as well as the boundary conditions. The collection of discrete boundary resistances can be represented as a vector:

$$\vec{R} = \left[R^1, R^2, \ldots, R^i, \ldots, R^{M_C}\right] \tag{4}$$

The decomposition of the structure into layers of different sizes allows the solution of the three-dimensional heat conduction equation in each layer ($k = 1, 2, \ldots, N_L$) to obtain solutions as Fourier series satisfying conditions (1) and (3). The as developed solutions are presented in Section 2.2. Next, an algorithm, described in Section 2.3, has been set up to assemble the temperature distributions of the different layers by applying continuity at contact boundaries in order to find, step by step, the heat flux and resistance vectors (2) and (4) for $k = 1, 2, \ldots, N_L$. Finally, temperature can be found at any point of the structure. In the case of perfect contact between layers, the vector relations (5) and (6) are used for such assembling:

$$\vec{T}_{k-1}|_{\text{bottom}} = \vec{T}_k|_{\text{top}} \tag{5}$$

$$\vec{\Phi}_{k-1}|_{\text{bottom}} = \vec{\Phi}_k|_{\text{top}} \tag{6}$$

Relations (5) and (6) mean that temperature-heat flux at the bottom and top faces of the respectively $(k-1)$-th and k-th layer are equal for each boundary element. In the case of non-perfect contact between layers, the relation (5) must be replaced by (7) for assembling:

$$\vec{T}_{k-1}|_{\text{bottom}} = \vec{T}_k|_{\text{top}} + \vec{R}_c \cdot \vec{\Phi}_k|_{\text{top}} \tag{7}$$

Each element of the vector $\vec{R}_c$, expressed in K W^{-1}, is the local thermal contact resistance referring to the boundary.

According to assumptions mentioned above, the vector $\vec{\Phi}_1$ is prescribed (top side of the structure). As the distribution $\vec{R}$ is found, bottom face heat flux is therefore determined by Eq. (3).

2.2. Solution of the heat conduction equation for any layer

This section gives the solution of the heat conduction equation for any homogeneous layer exposed to conditions (1) and (3). Subscript k, referring to the as-considered layer, is omitted in all quantities. Layer dimensions are L_x and L_y in the x- and y-directions respectively. The solution of the tridimensional heat conduction equation (8):

$$\nabla^2 T = 0 \tag{8}$$

satisfying the edge boundary conditions (9):

$$\left.\frac{\partial T}{\partial x}\right|_{x=0,L_x} = 0, \qquad \left.\frac{\partial T}{\partial y}\right|_{y=0,L_y} = 0 \tag{9}$$

can be expressed as a Double Fourier series as (see [10]):

$$T(x, y, z) = \sum_{n=0}^{N}\sum_{m=0}^{M} \tilde{\theta}(n, m, z)\frac{\cos(\alpha_n x)\cos(\beta_m y)}{N_{n,m}} \tag{10}$$

N, M are the truncation orders of the expansion series, $N_{n,m}$ is the norm of the scalar product:

$$N_{n,m} = \int_{x'=0}^{L_x}\int_{y'=0}^{L_y} \cos^2(\alpha_n x')\cos^2(\beta_m y')\,dx'\,dy' \tag{11}$$

with α_n, β_m the eigenvalues:

$$\alpha_n = \frac{n\pi}{L_x}, \qquad \beta_m = \frac{m\pi}{L_y} \tag{12}$$

and $\tilde{\theta}$ the Cosine Transform of $T(x, y, z)$ defined as:

$$\tilde{\theta}(n, m, z) = \int_{x'=0}^{L_x}\int_{y'=0}^{L_y} T(x', y', z')\cos(\alpha_n x')\cos(\beta_m y')\,dx'\,dy' \tag{13}$$

$\tilde{\theta}$ is the solution of the following matrix system (the subscripts *top*, *bottom* and ∞ refer respectively to the top and bottom faces of the layer and to the bottom side of the structure) obtained after applying the Fourier Transform (13) to the relations (1), (3) and (8) (see Appendix A):

$$\begin{bmatrix} \tilde{\theta}_{\text{top}} \\ \tilde{\Phi}_{\text{top}} \end{bmatrix} = \begin{bmatrix} A & B \\ C & D \end{bmatrix} \begin{bmatrix} I & \tilde{R}_{\text{bottom}} \\ 0 & I \end{bmatrix} \begin{bmatrix} \tilde{\theta}_{\infty} \\ \tilde{\Phi}_{\infty} \end{bmatrix} \tag{14}$$

with

$$\tilde{\theta} = [\tilde{\theta}_{0,0} \leftrightarrow \tilde{\theta}_{N,0} \cdots \tilde{\theta}_{0,m} \leftrightarrow \tilde{\theta}_{N,m} \cdots \tilde{\theta}_{0,M} \leftrightarrow \tilde{\theta}_{N,M}]^t \tag{15}$$

and

$$\tilde{\Phi} = [\tilde{\Phi}_{0,0} \leftrightarrow \tilde{\Phi}_{N,0} \cdots \tilde{\Phi}_{0,m} \leftrightarrow \tilde{\Phi}_{N,m} \cdots \tilde{\Phi}_{0,M} \leftrightarrow \tilde{\Phi}_{N,M}]^t \tag{16}$$

A, B, C and D are square diagonal matrices:

$$A = \text{diag}(A_{0,0} \leftrightarrow A_{N,0} \cdots A_{0,m} \leftrightarrow A_{N,m} \cdots A_{0,M} \leftrightarrow A_{N,M}) \tag{17}$$

with

$$A_{n,m} = \cosh(\gamma_{n,m} e) \tag{18}$$

B, C and D are calculated the same way with:

$$B_{n,m} = \cosh(\gamma_{n,m} e), \quad C_{n,m} = \lambda \gamma_{n,m} \sinh(\gamma_{n,m} e)$$
$$D_{n,m} = \cosh(\gamma_{n,m} e) \tag{19}$$

$\gamma_{n,m}$ depends on the eigenvalues α_n, β_m and is given by:

$$\gamma_{n,m}^2 = \alpha_n^2 + \beta_m^2 \tag{20}$$

I and $\tilde{R}_{\text{bottom}}$ are respectively the unit and convolution matrices of order $(N+1)(M+1) \times (N+1)(M+1)$. The calculation of the elements of $\tilde{R}_{\text{bottom}}$, a function of the resistance distribution $\vec{R}$, is detailed in Appendix A. Finally, the spectrum of the top temperature vector can be expressed as a function of the top heat flux vector by inverting a matrix of order $(N+1)(M+1) \times (N+1)(M+1)$ (see Appendix A). After calculating the spectra, the return to real space is carried out by the formula (10).

2.3. Solutions assembling

This section describes the algorithm set up for solutions assembling to find vectors $\vec{R}_k$ and $\vec{\Phi}_k$ at all boundaries ($k = 1$–N).

(x_k^i, y_k^i, e_k) and $(x_{k+1}^i, y_{k+1}^i, 0)$ are coordinates of the discrete element i for the k-th and $(k+1)$-th layers respectively and $R_C^{i,k}$, the contact resistance for the i-th discrete element between the k-th and $(k+1)$-th layers. According to Eq. (3) the k-th resistance vector is calculated as:

$$R_k(x_k^i, y_k^i, e_k) = \frac{T_k(x_k^i, y_k^i, e_k) - T_\infty}{\Phi_k(x_k^i, y_k^i, e_k)} \tag{21}$$

Because of the continuity of the temperature and the heat flux at the boundary between the k-th and $(k+1)$-th layers, Eq. (21) can be written as:

$$R_k(x_k^i, y_k^i, e_k) = \frac{T_{k+1}(x_{k+1}^i, y_{k+1}^i, 0) - T_\infty}{\Phi_{k+1}(x_{k+1}^i, y_{k+1}^i, 0)} \tag{22}$$

A temperature drop is created at the boundary by introducing the contact resistance:

$$R_k(x_k^i, y_k^i, e_k) = R_C^{i,k}(x_k^i, y_k^i, e_k) + \frac{T_{k+1}(x_{k+1}^i, y_{k+1}^i, 0) - T_\infty}{\Phi_{k+1}(x_{k+1}^i, y_{k+1}^i, 0)} \tag{23}$$

As mentioned above, a contact resistance can be taken into account at any point between layers.

The principle of the algorithm is indicated in Fig. 3. It is based on the iterative calculation of the resistance vectors until convergence of the process by using relation (23). The iterative sequences start from a set of initial resistance vectors (formally the vectors $\vec{R}_k^0$ for $k = 1$ to $N_L - 1$). According to relation (23) resistance $\vec{R}_k^1$ can be then approximated by:

$$R_k^1(x_k^i, y_k^i, e_k) = R_C^{i,k}(x_k^i, y_k^i, e_k) + \frac{T_{k+1}^0(x_{k+1}^i, y_{k+1}^i, 0) - T_\infty}{\Phi_{k+1}^0(x_{k+1}^i, y_{k+1}^i, 0)} \tag{24}$$

The calculation loop is repeated until the criterions (25) or (26) are satisfied:

$$\boldsymbol{C_R} = \max\left[\left(\max\left(\frac{|R_k^{j+1}(x_k^i, y_k^i, e_k) - R_k^j(x_k^i, y_k^i, e_k)|}{R_k^j(x_k^i, y_k^i, e_k)} \text{ for } i = 1, \ldots, N_{x_k} \times N_{y_k}\right)\right) \text{ for } k = 1, \ldots, N-1\right] \leqslant \varepsilon_R \tag{25}$$

$$\boldsymbol{C_T} = \max\left[\left(\max\left(\frac{|T_k^{j+1}(x_k^i, y_k^i, 0) - T_k^j(x_k^i, y_k^i, 0)|}{T_k^j(x_k^i, y_k^i, 0)} \text{ for } i = 1, \ldots, N_{x_k} \times N_{y_k}\right)\right) \text{ for } k = 1, \ldots, N\right] \leqslant \varepsilon_T \tag{26}$$

$\boldsymbol{C_R}$ and $\boldsymbol{C_T}$ are parameters testing convergence of resistance and temperature vectors, respectively. ε_R and ε_T are constants as small as desirable achieving convergence, typically equal to 1×10^{-3}, max is the maximum element of the vectors, N_{x_k}, N_{y_k} are the subdivision numbers according to the x- and y-axis.

3. Performance of the method

The performance of the Discrete Boundary Resistance method is studied by considering a three-dimensional packaged device constructed with four layers of different sizes and three rectangular heat sources (a, b, c), as shown in Fig. 4. The power is dissipated at the top side of the device over the regions a, b and c. Imperfect contacts between layers are considered. Dimensions and thermal conductivity of materials are reported in Table 1. Dissipated power is given in Table 2.

3.1. The case of uniform contact between layers

Contact between layers is first considered as uniform. Thermal contact resistances referring to each boundary are indicated in Table 3.

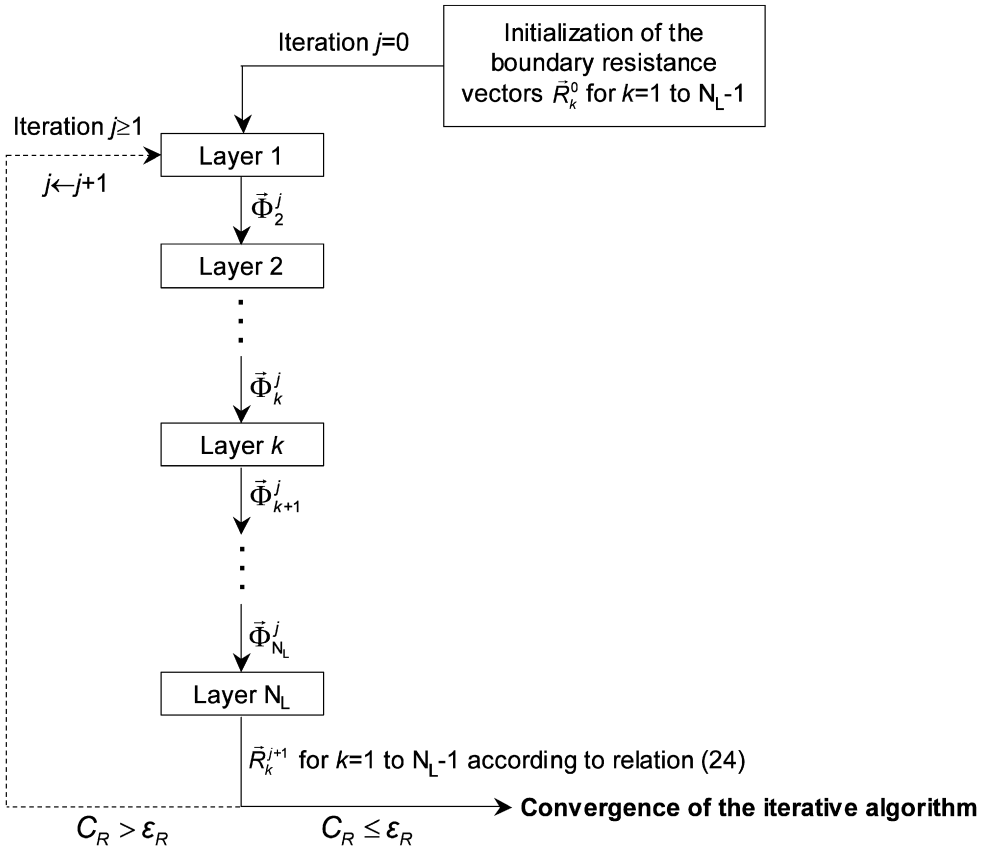

Fig. 3. Iterative assembling algorithm, as applied to the DBR method.

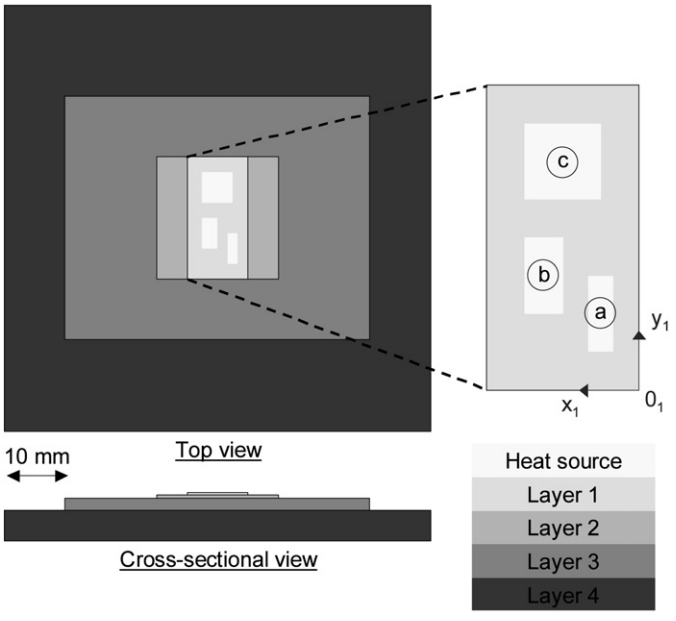

Fig. 4. Three-dimensional packaged device, as studied.

Table 1
Dimension and thermal conductivity of layers used in the device in Fig. 4

Layer	Thermal conductivity λ $W m^{-1} K^{-1}$	Length L_x mm	Length L_y mm	Thickness e mm
1	50	10	20	0.5
2	50	20	20	0.5
3	200	50	40	2
4	150	70	70	5

Table 2
Dimension of heat sources and dissipated power used in the device in Fig. 4

Heat source	Dissipated power W	Coordinate/x_1 mm	Coordinate/y_1 mm	Power density $W m^{-2}$
a	7.5	1.66–3.33	2.5–7.5	9×10^5
b	50	5–7.5	5–10	4×10^6
c	50	2.5–7.5	12.5–17.5	2×10^6

Table 3
Thermal contact resistance between layers used in the device in Fig. 4

Boundary	Thermal contact resistance R_C $K m^2 W^{-1}$
1	5×10^{-6}
2	5×10^{-6}
3	1×10^{-5}
4	1×10^{-4}

3.1.1. Temperature distribution

Fig. 5(a) shows the temperature distribution calculated at the top side of the device by the DBR method. The assembling algorithm was initialized by a constant boundary resistance equal to 1×10^{-4} $K m^2 W^{-1}$. Truncation orders for double Fourier Series were chosen to $N = M = 30$ in all layers. These results

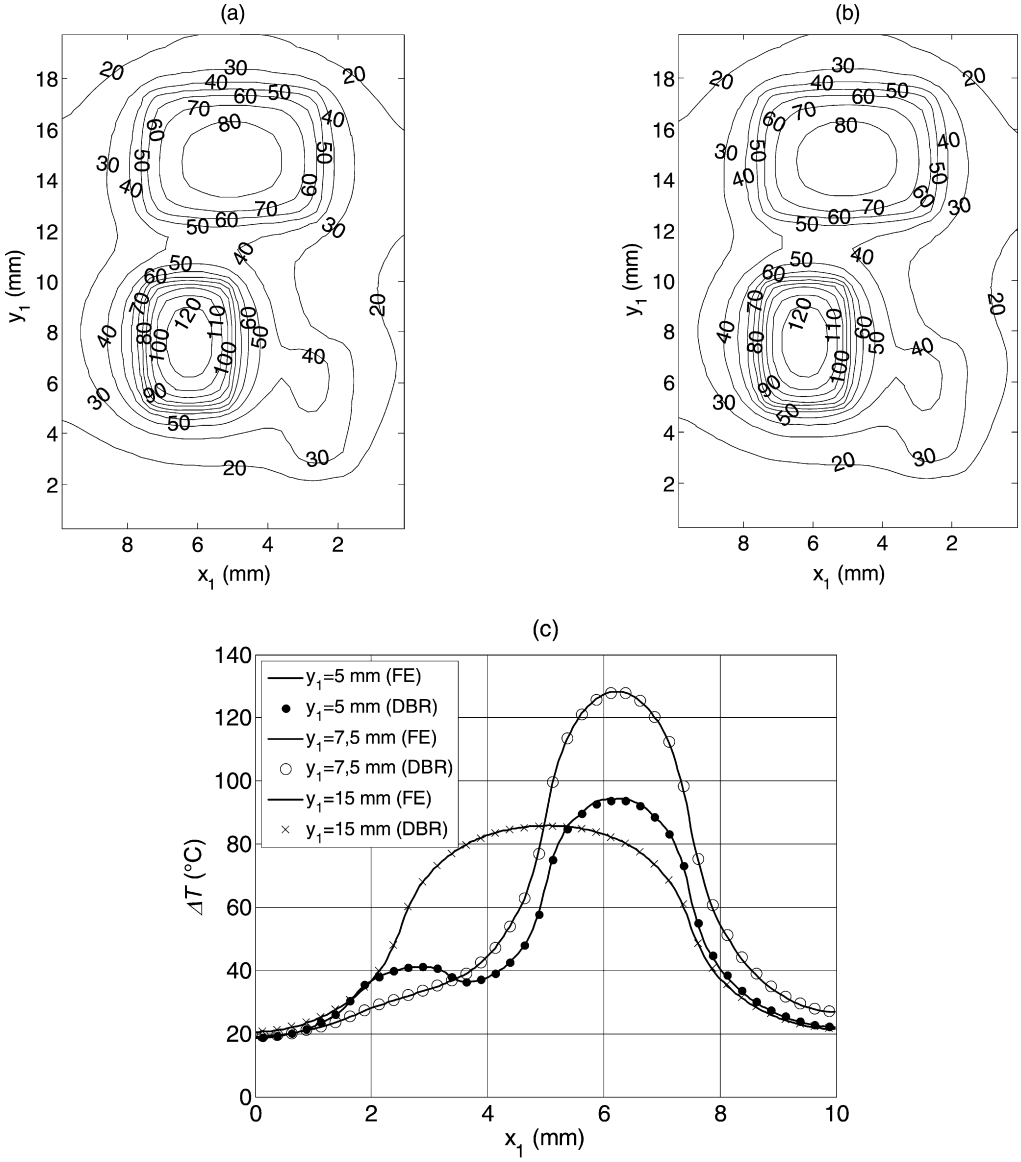

Fig. 5. Temperature distributions at the top side of the device (Fig. 4, Tables 1 and 2): (a) as calculated by the DBR method, (b) as calculated by the FEM software, (c) temperature profiles along the x-axis ($\Delta T = T_1 - T_\infty$).

were found in good agreement with the Finite-Element method (Comsol® – Multiphysics Software), as reported in Figs. 5(b) and 5(c). The difference between the methods does not exceed 1.5 °C over a regular grid of 20×40 points along the x_1 and y_1 axes when the maximum temperature reaches 130 °C.

3.1.2. Analysis of the convergence

Convergence of the solution is analyzed with respect to the assembling algorithm. Fig. 6 shows the variation of $\boldsymbol{C_T}$ (relation (26)) as function of the iterative sequences. Fig. 7 shows the change in calculated temperature (maximum temperature and within the dissipation regions a, b, c) as a function of the iterative sequences. Fig. 8 gives the distribution of the boundary resistance computed for layer 1 for different sequences of the calculation loop (2, 5, 10, 20 iterations). Results reported in Fig. 6, Fig. 7 and Fig. 8 demonstrate the very fast convergence of the calculation. For $\varepsilon_T = 10^{-3}$, the convergence criterion

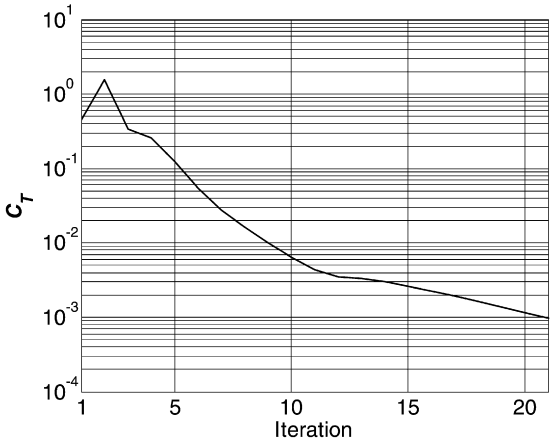

Fig. 6. Evolution of $\boldsymbol{C_T}$ as defined by relation (26) according to iterative sequences.

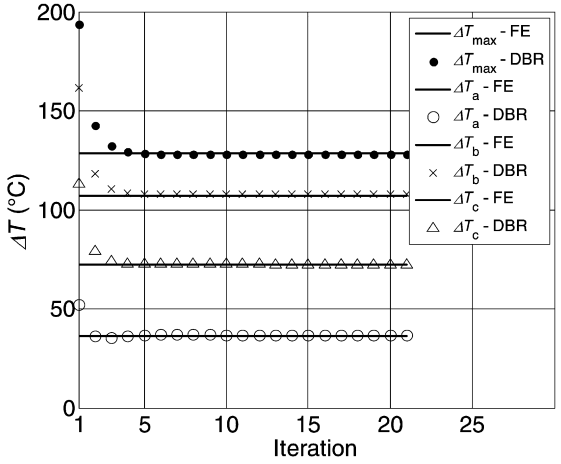

Fig. 7. Evolution of the calculated temperature at the top side of the device (maximum temperature $T_{\max}$ and heat source average temperatures $T_{\mathrm{a,b,c}}$ with $\Delta T = T - T_\infty$, FE: Finite-Elements, DBR: Discrete Boundary Resistance) according to iterative sequences.

$\boldsymbol{C_T} \leqslant \varepsilon_T$ is satisfied after 21 iterations (see Fig. 6). However, Fig. 7 shows that a couple of iterations are sufficient to calculate temperature with fine precision. 99.5% of the final value, calculated within the dissipation regions, is reached after only 5 iterations. One observes that resistance placed to the central region of the top layer (see Fig. 8) is rapidly calculated while ones near the edge slowly converge. Note that the lower resistance region can give the effective area of the heat flow. In a general way, lowest boundary resistance zones define the preferential paths of the heat flow across the full structure.

The accuracy of the method strongly depends on the truncation orders (N_k, M_k) of the Fourier series and the discretization orders (N_{x_k}, N_{y_k}) of the boundaries. Fig. 9 shows the influence of the truncation orders for $N_k = M_k$ and $k = 1, 2, 3, 4$ on the calculated temperature. One finds that high truncation orders are not required: the convergence is ensured with $N_k = M_k = 30$ for the maximum temperature and with $N_k = M_k = 20$ for the average temperature. Discretization orders have quite more significant influence (see Fig. 10). For the present case, boundaries are subdivided according to a regular square mesh and the temperature solution is found constant up to $N_{x_k} = N_{y_k} = 35$ for $k = 1, 2, 3, 4$. Generally, optimal truncation and discretization orders depend on layer dimensions and properties.

Influence of the initial boundary resistance set on the convergence is also investigated. The set, formally composed of the vector elements $\vec{R}_1^0$, $\vec{R}_2^0$ and $\vec{R}_3^0$ arbitrary chosen for each layer, has a strong impact on the convergence of iterative sequences, and consequently on the computational cost. A mismatch in convergence is observed on the variation of $\boldsymbol{C_T}$ as a function of the iterative sequences for different boundary resistance sets, as shown in Fig. 11. If the initial boundary resistance is lower than $1 \times 10^{-6}\ \mathrm{K\,m^2\,W^{-1}}$ then the algorithm does not systematically converge. The optimal set is achieved with an initial boundary resistance equal to $1 \times 10^{-4}\ \mathrm{K\,m^2\,W^{-1}}$. The computational cost can be drastically reduced by estimating initial values on the base of reasonable physical considerations. In a general way, initial sets of the boundary resistance vectors can be estimated by the following formula, obtained from a series 1-D thermal circuit:

$$R_k^0 = \sum_{j=k}^{3}\left(R_C^j + \frac{e_{j+1}}{\lambda_{j+1}}\right) + R_4 \quad \text{for } k = 1, \ldots, 3 \tag{27}$$

Fig. 12 shows the variation of $\boldsymbol{C_T}$ as a function of iterative sequences with the set given by the formula (27) for the three layers. Convergence is found after only 20 iterations which is not substantially different from results obtained with uniform initial boundary resistance sets equal to $1 \times 10^{-4}\ \mathrm{K\,m^2\,W^{-1}}$.

3.1.3. Computational time

All tests were performed with a 3 GHz, 1024 Mo Personal Computer.

Fig. 13 reports the temperature calculated by the DBR method at each iteration as a function of the computational time for the maximum and average temperature within the regions a, b, and c. Each iteration requires approximately 30 seconds. The time consumed, referred to the Finite-Element method, was evaluated for a suitable mesh of the full structure corresponding to a solution unchanged within 0.5% after meshing refinement. Fig. 13 demonstrates the higher performance of the DBR method with respect to the time consumed. The calculation by the Finite-Element method needs about 300 seconds, as indicated in Fig. 13, calculations performed with the DBR method are concluded after 150 seconds with a precision better than 0.5%.

3.2. The case of non-uniform contact between layers

Non-uniform contacts are then considered to test the method. Fig. 15 shows the temperature distributions calculated at the top of the device with a thermal contact between layers 1 and 2 exhibiting a non-uniform concentration of voids represented by function (28):

$$R_C^1(x_1, y_1) = 0.5 \times \sin(x_1 \cdot y_1) \tag{28}$$

R_C^1 is expressed in $\mathrm{K\,m^2\,W^{-1}}$. Function (28) is plotted in Fig. 14. As expected, the results reported in Fig. 15(a) and Fig. 15(c), using the DBR method, are in very good agreement with the results shown in Fig. 15(b) and Fig. 15(c), using the Finite-Element method. Maximum difference does not exceed 1.6 °C for a 20×40 point mesh. Impact of the region of high void concentration is clearly observed.

4. Conclusion

The Discrete Boundary Resistance method has been developed for determining temperature distribution in a semi-analytical way within tri-dimensional solid-state circuits and packaged devices in steady state conditions. The method is an interesting route to investigate complex structures with an arbitrary layout composed of multiple material layers and localized heat sources over sizes ranging from a fraction of a micron to a couple of centimeters.

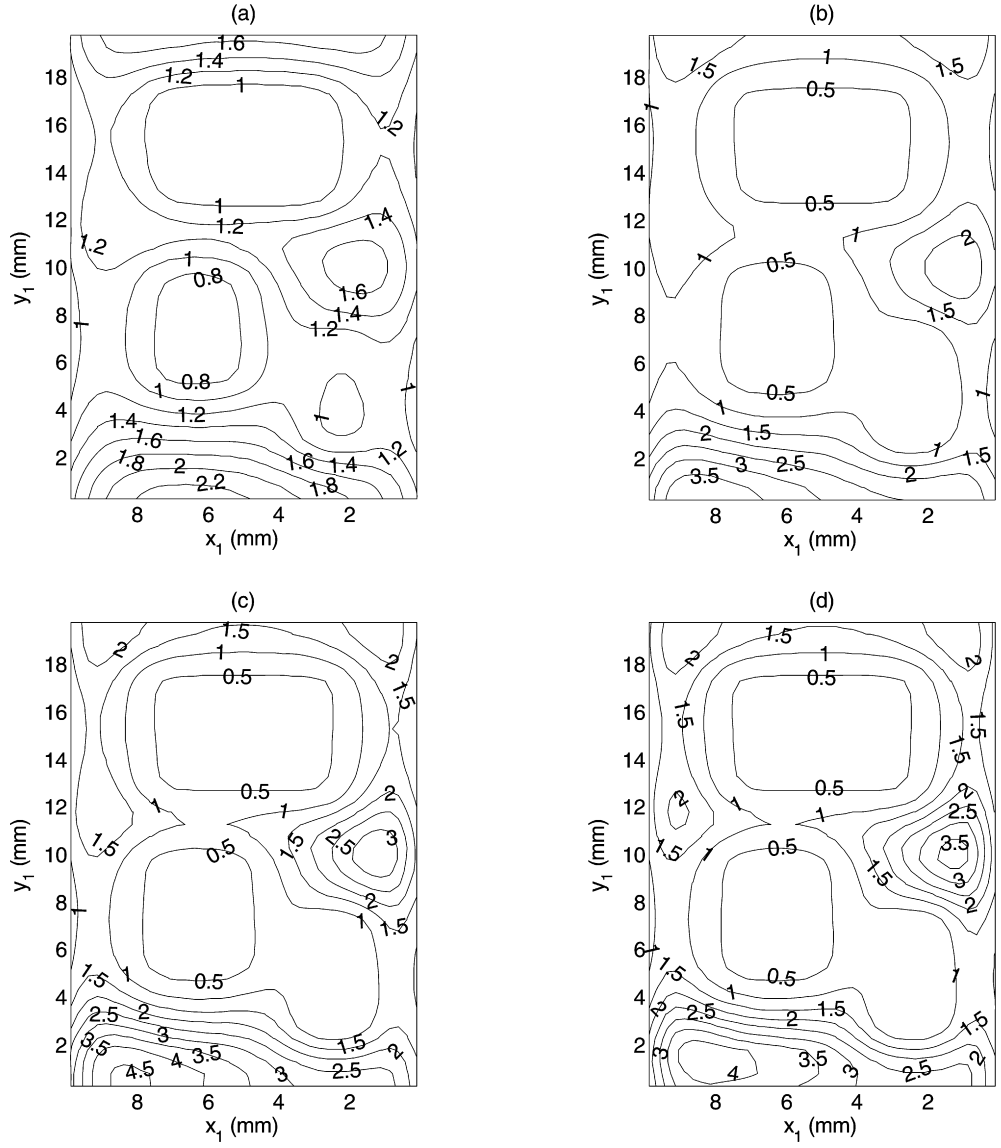

Fig. 8. Distribution of the Boundary Resistance (in 10^4 K m^2 W^{-1}), as calculated for the top layer: (a) after 2 iterations, (b) after 5 iterations, (c) after 10 iterations, (d) after 20 iterations.

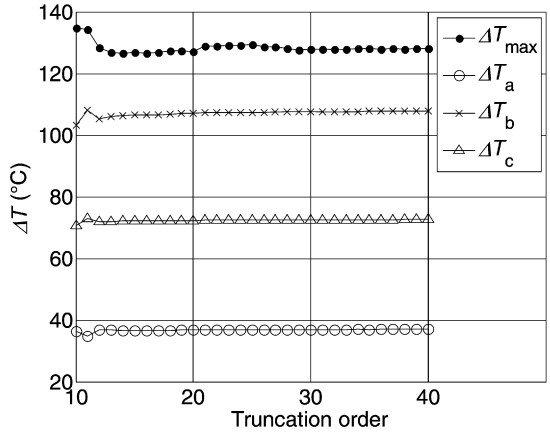

Fig. 9. Calculated temperature at the top side of the device (maximum temperature $T_{\max}$ and heat source average temperatures $T_{a,b,c}$ with $\Delta T = T - T_\infty$) as a function of the truncation order ($N_k = M_k$ for $k = 1, 2, 3, 4$).

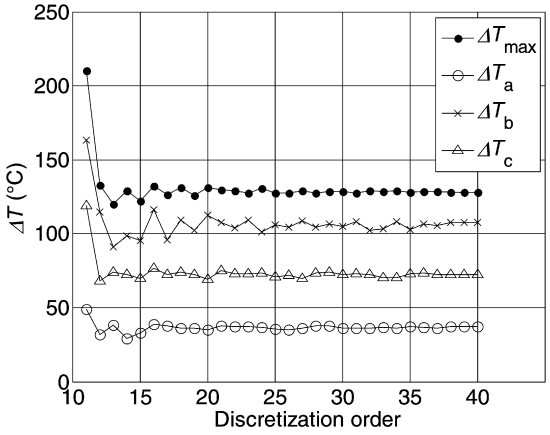

Fig. 10. Calculated temperature at the top side of the device (maximum temperature $T_{\max}$ and heat source average temperatures $T_{a,b,c}$ with $\Delta T = T - T_\infty$) as a function of the discretization order ($N_{x_k} = N_{y_k} = 35$ for $k = 1, 2, 3, 4$).

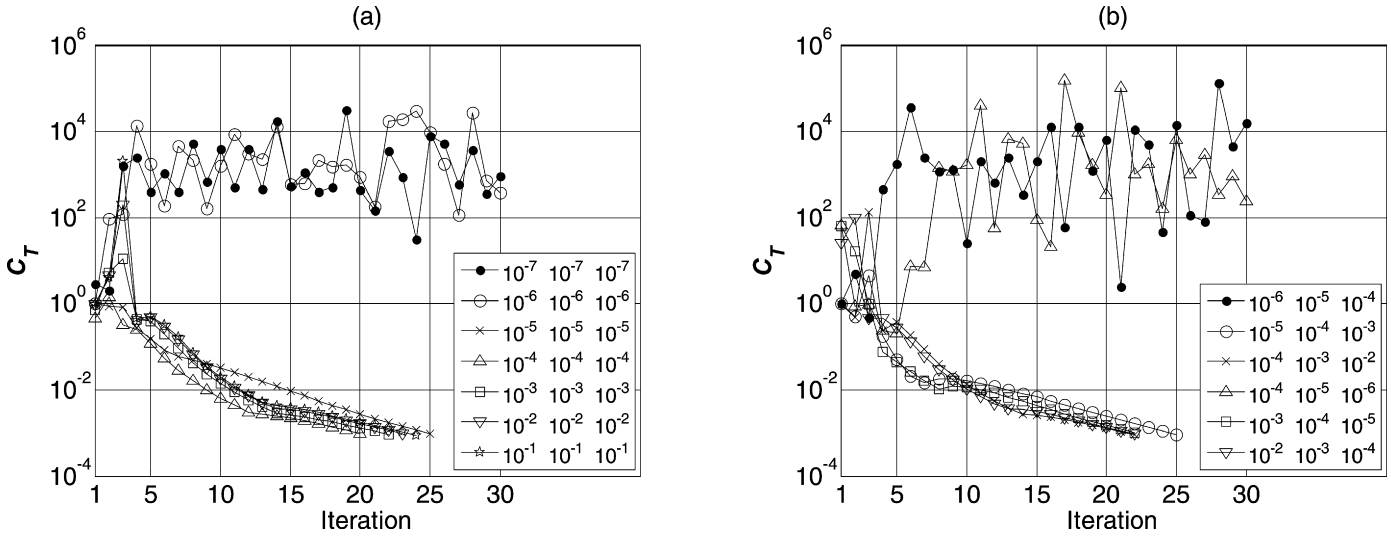

Fig. 11. Variation of C_T as a function of iterative sequences for different initial boundary resistance sets: (a) uniform sets, (b) non-uniform sets.

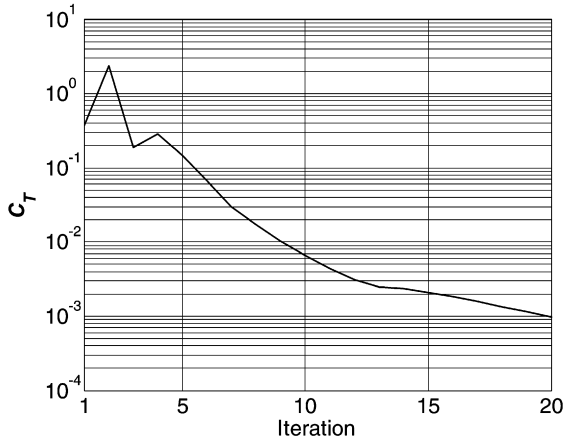

Fig. 12. Evolution of C_T according to iterative sequences for initial boundary resistance sets given by formula (27) ($R_1^0 = 1.73 \times 10^{-4}$, $R_2^0 = 1.58 \times 10^{-4}$, $R_3^0 = 1.43 \times 10^{-4}$ in K m^2 W^{-1}).

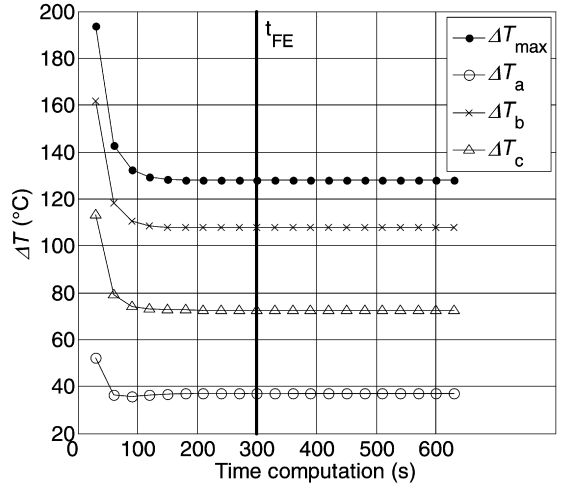

Fig. 13. Evolution of the calculated temperature at the top side of the device (maximum temperature T_{max} and heat source average temperatures $T_{a,b,c}$ with $\Delta T = T - T_\infty$) according to the computational time (t_{FE}: time consumed referred to the Finite-Element method).

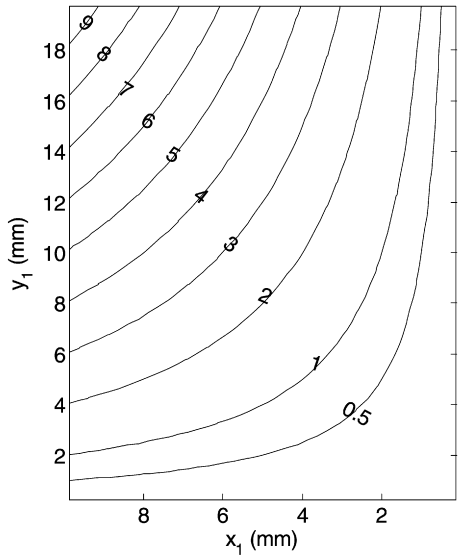

Fig. 14. Distribution of the thermal contact resistance between layers 1 and 2, as given by (28) ($R_C^1 \times 10^5$ K m^2 W^{-1}).

The method consists in decomposing the structure into layers of different sizes to develop for each one the solution of the heat conduction equation as a Double Fourier Series, after dividing the contact boundaries into discrete elements. The temperature solution is expressed as a function of a boundary resistance vector attached to the reference temperature of the full structure. An algorithm has been set up to assemble the temperature distributions of the different layers in order to find, step by step, the heat flux and resistance vectors at the boundaries.

The method has been studied in regards with a three-dimensional device constructed with multiple layers of different sizes and three rectangular heat sources. As expected, the method is found in very good agreement with the Finite-Element method, especially for non-uniform thermal contacts between layers. Efficiency of the assembling algorithm has been demonstrated in terms of accuracy and computational cost.

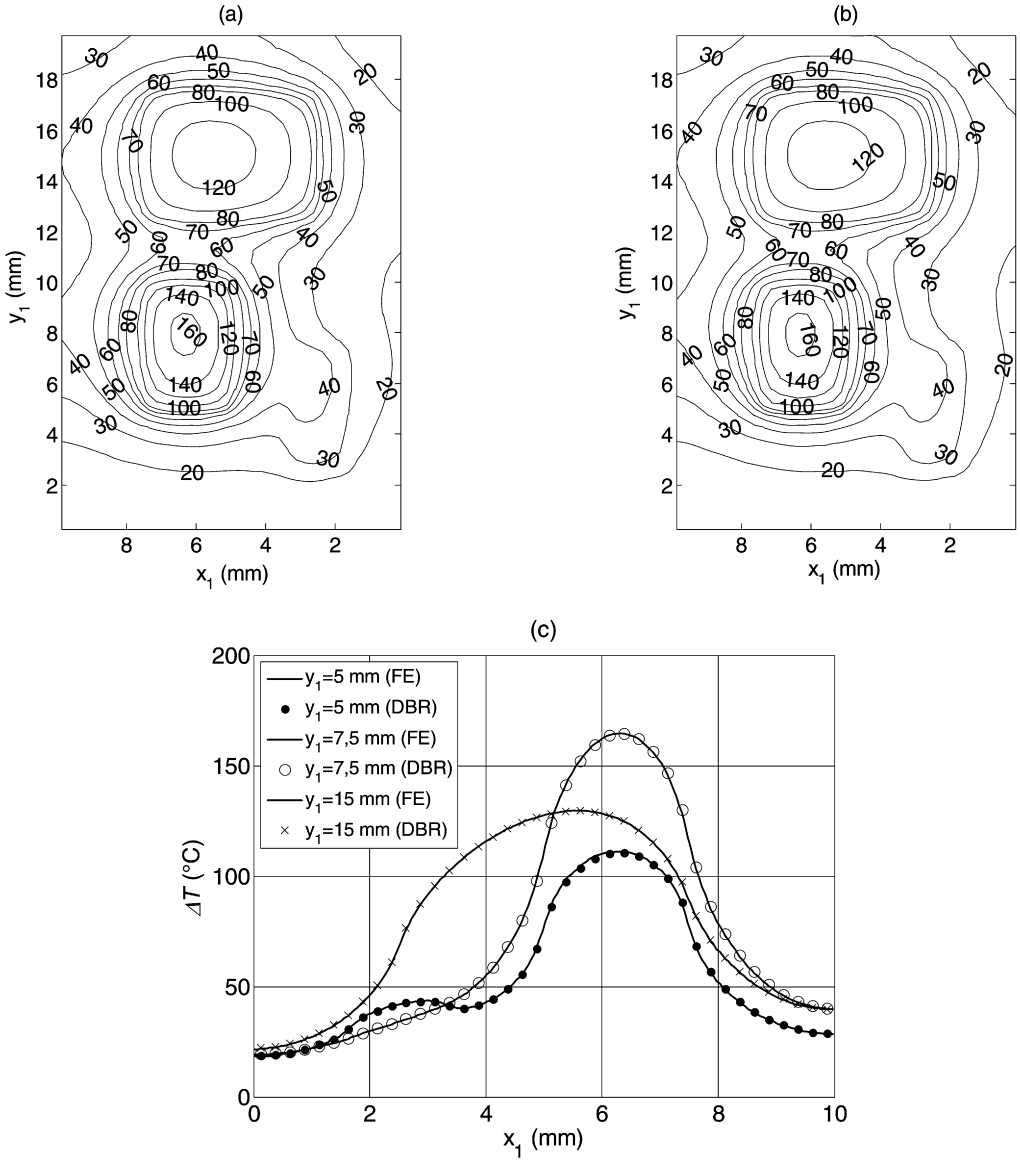

Fig. 15. Temperature distributions at the top side of the device (Fig. 4, Tables 1 and 2) with non-uniform thermal contact between layers 1 and 2: (a) as calculated by the DBR method, (b) as calculated by the FEM software, (c) temperature profiles along the x-axis ($\Delta T = T_1 - T_\infty$).

In addition, the convergence of the algorithm has been analyzed to find the optimal initial boundary resistance sets and the suitable truncation orders for series expansion and number of boundary elements.

Finally, the Boundary Resistance Method offers high precision and reasonable computational cost. This computational method is particularly attractive for analysis of compound semiconductor devices that have a strongly non-planar structure with large size range of components and high number of localized heat sources. The calculation of boundary resistance distributions can provide the preferential paths of heat flow through the structure. The method can be applicable to various complex circuits and devices. The next step of the development of the DBR method could consist in building a criterion that links the truncation and discretization orders for each layer in order to optimize the computational time and to reduce the number of hyper-parameters of the method. Also comparison with other semi-analytical methods [4,6,7] will be considered in the future. Additionally, the method could be extended to transient thermal analysis.

Supplementary material

The online version of this article contains additional supplementary material.

Please visit DOI: 10.1016/j.ijthermalsci.2008.05.011.

References

[1] Z. Radivojevic, K. Andersson, J.A. Bielen, P.J. van der Wel, J. Rantala, Operating limits for RF power amplifiers at high junction temperatures, Microelectronics Reliability 44 (2004) 963–972.

[2] M.P. Rodriguez, N.Y.A. Shammas, Finite element simulation of thermal fatigue in multilayer structures: thermal and mechanical approach, Microelectronics Reliability 41 (2001) 517–523.

[3] I. Guven, C.L. Chan, E. Madenci, Transient two-dimensional thermal analysis of electronic packages by the boundary element method, IEEE Transactions on Advanced Packaging 22 (3) (1999) 476–486.
[4] Z. Khatir, S. Lefebvre, Thermal analysis of high power IGBT modules, in: 12th International Symposium on Power Semiconductor Devices, Toulouse, 2000, pp. 271–274.
[5] J.V. Beck, K.D. Cole, A. Hadji-Sheikh, Heat Conduction Using Green Functions, Hemisphere, London, 1992.
[6] J.M. Dorkel, P. Tounsi, P. Leturcq, Three-dimensional thermal modeling based on the two-port network theory for hybrid or monolithic integrated power circuits, IEEE Transactions on Components, Packaging, and Manufacturing Technology, Part A 19 (4) (1996) 501–507.
[7] G. Maranzana, I. Perry, D. Maillet, Quasi-analytical simulation of conduction heat transfer through a pyramidal multilayer multiblock by the quadrupole method, Numerical Heat Transfer, Part B 42 (2002) 499–521.
[8] V. Feuillet, Y. Jarny, Y. Scudeller, Estimation of thermal resistance distributions for die-attach testing in microelectronics, Inverse Problems in Science and Engineering 15 (7) (2007) 715–742.
[9] P.E. Bagnoli, C. Bartoli, F. Stefani, Validation of the DJOSER analytical thermal simulator for electronic power devices and assembling structures, Microelectronics Journal 38 (2007) 185–196.
[10] D. Maillet, S. André, J.C. Batsale, A. Degiovanni, C. Moyne, Thermal Quadrupoles, Wiley, Chichester, 2000.